Polarimetric SAR Region Boundary Detection using B-spline Deformable Countours under the $\mathcal{G}^H$ Model

Juliana Gambini, Marta E. Mejail, Julio Jacobo-Berlles
Universidad de Buenos Aires
Facultad de Ciencias Exactas y Naturales
Departamento de Computación
Ciudad Universitaria, Pabellón I
C1428EGA Buenos Aires – República Argentina
{jgambini, marta, jacobo}@dc.uba.ar

Alejandro C. Frery
Universidade Federal de Alagoas
Departamento de Tecnologia da Informação
57072-970 Maceió, AL – Brazil
frery@tci.ufal.br

Abstract

In this paper a new approach to polarimetric Synthetic Aperture Radar (SAR) image region boundary detection is presented. It is based on a new model for polarimetric SAR data and the use of B-Spline active contours for image segmentation. In order to detect the boundary for a region, an initial B-Spline curve is specified and the proposed algorithm uses a deformable contours technique to find the boundary.

In doing this, the statistical parameters of the polarimetric $\mathcal{G}^H$ model for the data are estimated, in order to find the transition points between the region being segmented and the surrounding area.

This algorithm can be regarded as a local one, in the sense that it works on the region to be segmented instead of on the whole image

1 Introduction

The importance of polarimetric SAR images is due to the large amount of information they convey. References [4, 18, 20] show the potential of polarimetric SAR images compared to monopolarized SAR images in various applications.

Region boundary finding is an important task in image analysis, and many techniques have been proposed to solve this problem. In the particular case of polarimetric Synthetic Aperture Radar (SAR) images many techniques have been proposed for feature extraction and area classification (see [5, 12, 13, 23]), but they had never been combined with B-Spline based deformable contour methods. These methods have the advantage of operating on regions instead of over the whole image. Given the complexity of polarimetric SAR images this is a considerable advantage.

The B-spline approach has been widely used in curve representation for boundary detection [3], shape approximation [14] and object tracking [2]. Contours formulated by means of B-splines allow local control, have local representation, require few parameters and are intrinsically smooth.

The technique proposed in this work is based on B-Spline boundary fitting as considered by [1] tailored to the properties of polarimetric SAR imagery by means of the polarimetric $\mathcal{G}^H$ distribution as a general data model. The polarimetric $\mathcal{G}^H$ model was recently developed in [10] and presents an attractive choice for polarimetric SAR data segmentation.

This proposal for boundary extraction begins with the manual specification of initial regions of interest determined by a series of control points which generate a B-spline curve. Then, a series of radial segments are drawn on the image, and image data around them are extracted. For each segment, the transition point, that is, the point belonging to the region boundary, is determined by parameter estimation from the data under the $\mathcal{G}^H$ model.

Then, for each region, the contour sought is given by the

B-spline curve that fits these transition points. In all that follows, random variables will be denoted by capital letters; for vectors and matrices bold characters will be used. The structure of this paper is as follows: section 2 describes the statistical model used for monopolarimetric SAR data, section 3.1 presents the statistical model for polarimetric SAR data, section 4 gives an introduction to B-Spline curve fitting, section 5 specifies the criterion used to determine the transition points and explains the region fitting algorithm, section 6 shows the obtained results and section 7 presents the conclusions.

2 The $\mathcal{G}$ distribution for monopolarized SAR data

The multilook return in monopolarized SAR images can be modeled as the product of two independent random variables, one corresponding to the backscatter X and other to the speckle noise Y. In this manner

$$Z = X \cdot Y \tag{1}$$

models the return Z in each pixel under the multiplicative model. For monopolarized data, the speckle noise Y is modeled as a $\Gamma(n, n)$ distributed random variable, where n is the number of looks, while the backscatter X is considered to obey a Generalized Inverse Gaussian law, denoted as $\mathcal{N}^{-1}(\alpha, \lambda, \gamma)$ (see [22]).

For particular values of the parameters of the $\mathcal{N}^{-1}$ distribution, the $\Gamma(\alpha, \lambda)$, the $\Gamma^{-1}(\alpha, \gamma)$, and the $IG(\gamma, \lambda)$ (Inverse Gaussian) distributions are obtained. These, in turn, give rise to the K, the $\mathcal{G}^0$, and the $\mathcal{G}^H$ distributions for the return Z, respectively.

The IG distribution can be reparametrized according to

$$\begin{aligned} \omega = &\quad \sqrt{\lambda\gamma}, \\ \eta = &\quad \sqrt{\lambda/\gamma}. \end{aligned}$$

With this parametrization, η is the mean vaule and ω represents the variability of the backscatter.

Given the mathematical tractability and descriptive power of the $\mathcal{G}^0$ (see [11, 15, 16, 17, 19]) and the $\mathcal{G}^H$ distributions, they represent an attractive choice for SAR data modeling.

The density functions for these models are given by

$$f_{\mathcal{G}^0}(z) = \frac{2n^n\Gamma(n-\alpha)}{\gamma^\alpha\Gamma(-\alpha)\Gamma(n)} \cdot \frac{z^{2n-1}}{(\gamma + z^2 n)^{n-\alpha}}, \tag{2}$$

where $-\alpha, \gamma, z > 0$ and $n \geq 1$, and

$$f_{\mathcal{G}^H}(z) = \frac{n^n}{\Gamma(n)}\sqrt{\frac{2\omega\eta}{\pi}}e^\omega\Big(\frac{\omega}{\eta(\omega\eta + 2nz)}\Big)^{n/2+1/4} \cdot z^{n-1}K_{n+1/2}\Big(\sqrt{\frac{\omega}{\eta}(\omega\eta + 2nz)}\Big), \tag{3}$$

with $\omega, \eta, z > 0$ and $n \geq 1$, respectively.

The moments of the $\mathcal{G}^0$ and the $\mathcal{G}^H$ distributions are:

$$E_{\mathcal{G}^0}(Z^r) = \Big(\frac{\gamma}{2n}\Big)^r \frac{\Gamma(-\alpha + r)}{\Gamma(-\alpha)} \frac{\Gamma(n + r)}{\Gamma(n)}, \qquad -\alpha > r, \tag{4}$$

and

$$E_{\mathcal{G}^H}(Z^r) = \Big(\frac{\eta}{n}\Big)^r e^\omega \sqrt{\frac{2\omega}{\pi}} K_{r-1/2}(\omega) \frac{\Gamma(n + r)}{\Gamma(n)}, \tag{5}$$

respectively, and are used to estimate the statistical parameters. The K_ν is the modified Bessel function of the third kind and order ν, whose integral representation is [8]:

$$K_\nu(z) = \int_0^\infty \exp\{-z\cosh(t)\}\cosh(\nu t)dt.$$

Numerical problems arise when computing this function [7], but the distribution used in this paper circumvents this issue as will be seen in the next section.

3 Polarimetric SAR Data

Polarimetric SAR systems use antennas designed to transmit and receive electromagnetic waves of a specific polarization, being the two most common polarizations the horizontal linear or H, and vertical linear or V. Due to the possible change in polarization of the scattered wave, radar antennas are often designed to receive the different polarization components simultaneously and, therefore, HH, VV, HV and VH data will be available in a full polarimetric system. HV and VH channels are strongly correlated, so one will be discarded in the following.

We will follow the multiplicative paradigm, sothe returned data will be considered as the result of the product between backscatter and speckle, given by

$$\begin{bmatrix} Z_{hh} \\ Z_{hv} \\ Z_{vv} \end{bmatrix} = \sqrt{X} \begin{bmatrix} Y_{hh} \\ Y_{hv} \\ Y_{vv} \end{bmatrix}, \tag{6}$$

where $\mathbf{Z} = [Z_{hh}, Z_{hv}, Z_{vv}]^t$ and $\mathbf{Y} = [Y_{hh}, Y_{hv}, Y_{vv}]^t$ are complex random vectors modelling, respectively, the returned signal and the speckle noise; the random variable X is a scalar that models backscatter variability due to the heterogeneity of the sensed area.

We define now the 3×3 complex random matrix $\mathbf{Z}^{(n)}$, given by

$$\mathbf{Z}^{(n)} = \frac{1}{n}\sum_{k=1}^{n} \mathbf{Z}(k)\mathbf{Z}^{*t}(k), \tag{7}$$

where n is the number of looks and $\mathbf{Z}(k)$ are complex random variables that correspond to each of the n looks. In a

similar way, we can also define $\mathbf{Y}^{(n)}$ as

$$\mathbf{Y}^{(n)} = \frac{1}{n}\sum_{k=1}^{n}\mathbf{Y}(k)\mathbf{Y}^{*t}(k), \tag{8}$$

for the speckle noise. Then, from (6), (7) and (8) one has

$$\mathbf{Z}^{(n)} = X\mathbf{Y}^{(n)}, \tag{9}$$

so equation (6) can be rewritten as

$$\mathbf{Z}^{(n)} = \frac{X}{n}\sum_{k=1}^{n}\mathbf{Y}(k)\mathbf{Y}^{*t}(k) \tag{10}$$

where

$$\mathbf{Y}(k)\mathbf{Y}^{*t}(k) = \begin{bmatrix} |Y_{hh}(k)|^2 & Y_{hh}(k)Y_{hv}^*(k) & Y_{hh}(k)Y_{vv}^*(k) \\ Y_{hh}^*(k)Y_{hv}(k) & |Y_{hv}(k)|^2 & Y_{hv}(k)Y_{vv}^*(k) \\ Y_{hh}^*(k)Y_{vv}(k) & Y_{hv}^*(k)Y_{vv}(k) & |Y_{vv}(k)|^2 \end{bmatrix}. \tag{11}$$

In the folowing subsections we explain the polarimetric version of the $\mathcal{G}^H$ distribution.

3.1 A polarimetric version of the $\mathcal{G}^H$ distribution

If we consider that the components of $\mathbf{Y}(k)$ exhibit a Multivariate Complex Gaussian distribution, then $n\mathbf{Y}^{(n)}$ will have a Centered Complex Wishart distribution (see [6]), so the density function of $\mathbf{Y}^{(n)}$ will given by

$$f_{\mathbf{Y}^{(n)}}(\mathbf{y}) = \frac{n^{3n}\,|\mathbf{y}|^{n-3}}{\pi^3\Gamma(n)\cdots\Gamma(n-2)\,|\mathbf{\Sigma_Y}|^n}\cdot \exp(-n\mathrm{Tr}(\mathbf{\Sigma_Y}^{-1}\mathbf{y})), \tag{12}$$

for $n \geq 3$ and for $\mathbf{Y} \in \mathbb{C}^{3\times 3}$, where Tr is the trace operator, $|\cdot|$ denotes the determinant of a matrix and $\mathbf{\Sigma_Y}$ is the covariance matrix of $\mathbf{Y}$.

In order to find the density function of $\mathbf{Z}^{(n)}$, the integral given by

$$f_{\mathbf{Z}^{(n)}}(\mathbf{z}) = \int_{\mathtt{R}_+} f_{\mathbf{Z}^{(n)}|X=x}(\mathbf{z})\, f_X(x)\, dx \tag{13}$$

is calculated. Using equation (12) it can be easily found that

$$f_{\mathbf{Z}^{(n)}|X=x}(\mathbf{z}) = x^{-3^2} f_{\mathbf{Y}^{(n)}}(x^{-1}\mathbf{z}). \tag{14}$$

We will consider that the variability of backscatter, modeled by random variable X, will follow a Inverse Gaussian distribution with unitary mean. So, its density function f_X will be given by

$$f_X(x) = \sqrt{\frac{\omega}{2\pi x^3}}\exp\Big(-\frac{1}{2}\omega\frac{(x-1)^2}{x}\Big)\,\mathbf{1}_{\mathbb{R}^+}(x), \tag{15}$$

where

$$\mathbf{1}_A(x) = \begin{cases} 1 & \text{if } x \in A \\ 0 & \text{if } x \notin A \end{cases} \tag{16}$$

and ω is a roughness parameter. Now, from formulæ (13), (14) and (15) we can finally write $f_{\mathbf{Z}^{(n)}}$ as

$$f_{\mathbf{Z}^{(n)}}(\mathbf{z}) = \frac{\sqrt{\frac{2}{n}}n^{3n}e^{\omega}\omega^{3n+1}\,|\mathbf{z}|^{n-3}}{\pi^3\Gamma(n)\cdots\Gamma(n-2)\,|\mathbf{\Sigma_Y}|^n}\cdot \frac{K_{3n+1/2}(\sqrt{\omega(2n\mathrm{Tr}(\mathbf{\Sigma_Y}^{-1}\mathbf{z})+\omega)})}{(\omega(2n\mathrm{Tr}(\mathbf{\Sigma_Y}^{-1}\mathbf{z})+\omega))^{\frac{3}{2}n+\frac{1}{4}}}. \tag{17}$$

The Bessel function $K_{3n+1/2}$ above can be computed using a closed formula:

$$K_{np+1/2}(\nu) = \sqrt{\frac{\pi}{2\nu}}e^{\nu}\sum_{k=0}^{np}\frac{(np+k)!}{k!(np-k)(2\nu)^k}, \tag{18}$$

with

$$\nu = \sqrt{\omega(2n\mathrm{Tr}(\mathbf{\Sigma_Y}^{-1}\mathbf{z})+\omega)}, \tag{19}$$

alleviating, thus, the numerical issues that the evaluation of this function imposes in the general case.

Figure 1 shows a synthetic image with this distribution. A similar approach had been used in [9] for parameter estimation of the two-channel sample covariance matrix, assuming an inverse χ^2 distribution.

3.2 Parameter Estimation

The estimation of the roughness parameter ω is done using the first and second order moments of of the diagonal elements of $\mathbf{Z}^{(n)}$ (see [10]). The components of the principal diagonal of $\mathbf{Z}^{(n)}$, are given by

$$Z_{i,i}^{(n)} = \frac{X}{n}\sum_{k=1}^{n}|Y_{k,i}|^2\,, \text{with } i \in \{hh, hv, vv\}\,,$$

where the random variables X and $n^{-1}\sum_{k=1}^{n}|Y_{k,i}|^2$ are such that $X \sim GI(\omega,1)$ and $n^{-1}\sum_{k=1}^{n}|Y_{k,i}|^2 \sim \sigma_i^2\Gamma(n,2n)$. This is equivalent to considering $Z_{i,i}^{(n)}$ as the result of the product of a $GI(\omega,\sigma_i^2)$ distributed random variable and a $\Gamma(n,2n)$ distributed random variable, because a $\sigma_i^2 GI(\omega,1)$ distributed random variable is $GI(\omega,\sigma_i^2)$ distributed. This, in turn, implies that $Z_{i,i}^{(n)}$ is a $G_I^H(\omega,\sigma_i^2,n)$ distributed random variable.

Given the independence between the random variables X and Y, the rth-order moment of Z is obtained multiplying the rth-order moments of Y and X. The rth-order moment of X is

$$\mathbb{E}\left[X^r\right] = \sqrt{\frac{2\omega}{\pi}}e^{\omega}\eta^r K_{r-\frac{1}{2}}(\omega) \tag{20}$$

and the rth-order moments of Y is

$$\mathbb{E}[Y^r] = \frac{1}{n^r}\frac{\Gamma(n+r)}{\Gamma(n)} \tag{21}$$

Then, the rth-order moment of the return Z is

$$\mathbb{E}[Z^r] = (\frac{\eta}{n})^r e^{\omega}\sqrt{\frac{2\omega}{\pi}}K_{r-\frac{1}{2}}(\omega)\frac{\Gamma(n+r)}{\Gamma(n)} \tag{22}$$

Then, calling

$$m_{1i} = \mathbb{E}[Z_{i,i}^{(n)}]$$

and

$$m_{2i} = \mathbb{E}[(Z_{i,i}^{(n)})^2]$$

the estimates of ω are given by

$$\widehat{\omega}_i = \frac{1}{\frac{n}{n+1}\frac{m_{2i}}{m_{1i}^2} - 1}, \tag{23}$$

for $i \in \{HH, HV, VV\}$. We adopt the average of these three values as the estimated value for the parameter ω:

$$\widehat{\omega} = \frac{\widehat{\omega}_1 + \widehat{\omega}_2 + \widehat{\omega}_3}{3}. \tag{24}$$

3.3 Parameter interpretation

One of the most important features of the $\mathcal{G}^H$ distribution is that the estimated values of the parameter ω have immediate interpretation in terms of roughness. For values of ω near zero, the imaged area presents very heterogeneous gray values, as is the case of urban areas in polarimetric SAR images. As we move to less heterogeneous areas like forests, the value of ω grows, reaching its highest values for homogeneous areas like pastures and certain types of crops. This is the reason why this parameter is regarded to as a roughness or texture measure.

4 B-spline Representation

In this work, the B-spline curve representation for describing object contours in an scene is used. B-splines are a convenient representation of spline functions with the following interesting features:

1. The curve is represented by a few parameters, the control points; this reduces the computational effort to compute it.

2. The order of the polynomial segments is chosen arbitrarily, and it relates to the desired smoothness.

3. The B-spline approach allows the local control of the curve by controlling the control points individually.

4. The curve lies within the convex hull induced by the control points.

In the following, a brief review of B-spline representation of contours is presented; for more details see the works [1, 21].

Let $\{Q_0, \ldots, Q_{N_B-1}\}$ be a set of control points, where $Q_n = (x_n, y_n)^t \in \mathbb{R}^2$, $0 \leq n \leq N_B - 1$, and let $\{s_0 < s_1 < s_2 < \cdots < s_{L-1}\} \subset \mathbb{R}$ be a set of L knots. A B-spline curve of order d is defined as a weighted sum of N_B polynomial basis functions $\mathrm{B}_{n,d}(s)$ of degree $d-1$, within each interval $[s_i, s_{i+1}]$ with $0 \leq i \leq L-1$. The constructed spline function is $r(s) = (x(s), y(s))^t$, $0 \leq s \leq L-1$, being

$$r(s) = \sum_{n=0}^{N_B-1} \mathrm{B}_{n,d}(s)Q_n,$$

and

$$x(s) = \mathrm{B}^t(s)Q^x \tag{25}$$

$$y(s) = \mathrm{B}^t(s)Q^y \tag{26}$$

where the basis functions vector $\mathrm{B}(s)$ of N_B components is given by $\mathrm{B}(s) = (\mathrm{B}_{0,d}(s), \ldots, \mathrm{B}_{N_B-1,d}(s))^t$. The weight vectors Q^x and Q^y give the first and second components of Q_n, respectively.

The curves used in this work are closed, with $d = 3$ or $d = 4$, and are specified by periodic B-spline basis functions.

We now present a brief review of the problem of determining a polygon that generates a fitting B-spline curve with known number of control points, N_B.

Consider $\{D_0, D_1, \ldots, D_{k-1}\} \in \mathbb{R}^2$, k points in the image plane, where $D_i = (x_i, y_i)^t$, $i = 0, \ldots, k-1$; the spline curve that best fits them is sought. Equations (25) and (26), imply that the components D_i must satisfy

$$x_i = \mathrm{B}^t(t_i)Q^x,$$
$$y_i = \mathrm{B}^t(t_i)Q^y,$$

for certain values of t_i, where $i = 0, \ldots, k-1$, and $N_B \leq k$.

This linear system is more compactly written in matrix form as $D = K(Q^x \ Q^y)$, where the $k \times N_B$ elements of the real matrix K are given by $K_{ij} = B_{j,d}(t_i)$, with $i = 0, \ldots, k-1$, $j = 0, \ldots, N_B - 1$, and $D = (D_0, D_1, \ldots, D_k)^t$. In the most general case $N_B < k$ and, therefore, K is not a square matrix. In this case, the pseudo-inverse matrix form $(Q^x \ Q^y) = K^+D$ is used to find the B-spline fitting curve. A useful set of values for the parameters $\{t_0, \ldots, t_{k-1}\}$ is given by

$$t_0 = 0, \ t_\ell = \frac{\sum_{i=1}^{\ell}\|D_i - D_{i-1}\|}{\sum_{i=1}^{k-1}\|D_i - D_{i-1}\|}, \ell \geq 1.$$

The knot set to build the B-spline basis functions is arbitrarily chosen.

5 Boundary detection

In this section we describe an algorithm developed for boundary detection using B-spline deformable contours. Let E be a scene made up by the background B and a region R with its boundary ∂R. We want to find a curve C_B that fits ∂R in the image. We define an initial search area, which is specified by polygons, the vertexes of which are control points that generate a B-spline curve, as Figure 2 shows. Once the initial search zone is determined the centroid is calculated.

If a point belongs to the object boundary, then a sample taken from the neighborhood of that point should exhibit a change in the statistical parameters and it is considered to be a transition point. Then N segments $s^{(i)}$, $i = 1, \ldots, N$ of the form $s^{(i)} = \overline{CP_i}$ are considered, being C the centroid of the initial region, the extreme P_i a point outside of the region and being $\theta = \angle(s^{(i)}, s^{(i+1)})$ the angle between two consecutive segments, for every i. It is necessary for the centroid C to be in the interior of the object whose contour is sought.

The segment $s^{(i)}$ is an array of $m \times 6$ elements coming from a discretization of the straight line on the array of the polarimetric image and is given by:

$$s^{(i)} = \left(z_1^{(i)}, \ldots, z_m^{(i)}\right), \quad 1 \leq i \leq N.$$

where $z_k^{(i)}, k = 1, \ldots m$ is an array of 6 elements as Figure 3 shows.

For each segment $s^{(i)}$, $1 \leq i \leq N$, we consider the following partition

$$Z_k^{(i)} \sim \mathcal{G}^H(\omega_r), \quad k = 1, \ldots, j$$
$$Z_k^{(i)} \sim \mathcal{G}^H(\omega_b), \quad k = j+1, \ldots, m$$

where for each k, with $1 \leq k \leq m$, $z_k^{(i)}$ is the realization of the random variable $Z_k^{(i)}$. The parameters ω_r and ω_b characterize the region and its background, respectively.

In order to find the transition point on each segment $s^{(i)}$, the parameter ω is estimated as explained in section 3.1 using a rectangle around the segment and a sliding window of dimension 20×20. Then the $\hat{\Omega}^{(i)} = (\omega_1, \ldots, \omega_m)$ are obtained and the biggest variation of $\hat{\Omega}^{(i)}$ within the array is found convolving it with the mask $[-2, -1, 0, 1, 2]$. Once the set of border points $A = \{b_1, ..., b_N\}$ is found, the method builds the interpolating B-spline curve as its explained in section 4. Algorithm 1 shows a summary of the process to find the border points.

6 Results

A synthetic image, under the polarimetric $\mathcal{G}^H$ model, with two different regions was generated. The parameters are $\omega = 1.0$ for the object and $\omega = 10.0$ for the background, see Figure 1. In this work it was not necessary to consider the other nine parameters of the polarimetric data to detect the transition points, given the very good performance obtained using the estimation of the ω parameter alone.

Algorithm 1 Boundary Detect Algorithm

1: Determination of the region of interest using a B-Spline curve.
2: Determination of a series of radial segments on the image.
3: **for** each segment **do**
4: Estimation of statistical parameters for polarimetric SAR data, using the data within a rectangular window around the segment, as explained in section 3.1.
5: Detection of the border point by convolving with a border detection operator.
6: **end for**
7: Determination of the B-Spline that interpolates the points found.

Figure 4 shows the results of applying Algorithm 1 to this image. Figure 5 shows the probability of finding the border point with an error lower than the number of pixels indicated on the horizontal axis. This graph was generated using a Monte Carlo method, taking 200 samples of rectangular windows of synthetic polarimetric SAR data and calculating the transition point for each of them. Then, the relative frequency of finding the border with an error less than a number of pixels, is calculated.

Figure 6(a) shows typical values of the array $\hat{\Omega}^{(i)}$ for the segment $s^{(i)}$. Figure 6(b) shows the variation in the array $\hat{\Omega}^{(i)}$.

Figure 7(a) shows a 3 looks real E-SAR image showing an urban area from the city of Munich, while Figure 7(b) shows a region boundary detected using Algorithm 1. As can be seen, the technique deals well with both complex structures and noisy data.

7 Conclusions

In this paper, a new approach to region boundary detection in polarimetric SAR images using B-spline deformable contours is described. The boundaries of several regions with varying degrees of complexity were obtained using our proposal.

In the first step we find regions of interest that correspond to areas with different degrees of homogeneity, as a coarse first approximation. For each region, its respective boundaries are considered as the initial solution for the border detector. Then, the estimated parameter of roughness is calculated using two samples: one included in the region and the other out of the region and we find the transition

point only for the data that are on a set surround a line segments.

All these processes diminish the computational cost and improve the performance of the method.

For each region, the result of the application of this algorithm is a boundary curve given by an expression in terms of B-Spline functions. The results using both simulated and real SAR images are excellent and were obtained with an acceptable computational effort.

Future work includes the use of more parameters for finer detail detection.

8 Acknowledgements

We thank DLR for the E-SAR image provided.

References

[1] A. Blake and M. Isard. *Active Contours*. Springer Verlag, 1998.

[2] P. Brigger, J. Hoeg, and M. Unser. B-spline snakes: A flexible tool for parametric contour detection. *IEEE Transactions on Image Processing*, 9(9):1484–1496, Sept. 2000.

[3] R. Cipolla and A. Blake. The dynamic analysis of apparent contours. In *Proceedings of the 3rd Int. Conf. on Computer Vision*, pages 616–625, 1990.

[4] W. Dierking, H. Skriver, and P. Gudmandsen. SAR polarimetric for sea ice monitoring. In *ESA POlInSAR workshop, ESRIN*, 2003.

[5] L. Ferro-Famil and J. Lee. Unsupervised classification of multifrequency and fully polarimetric SAR images based on the H-A-Alpha-Wishart classifier. *IEEE Transactions on Geoscience and Remote Sensing*, 39:2332–2342, 2001.

[6] J. W. Goodman. *Sattistical Optics, Pure and Applied Optics*. Wiley, New York, USA, 1985.

[7] S. D. Gordon and J. A. Ritcey. Calculating the K-distribution by saddlepoint integration. *IEE Proceedings in Radar, Sonar and Navigation*, 142(4):162–165, August 1995.

[8] I. S. Gradshteyn and I. M. Ryzhik. *Table of Integrals, Series and Products*. Academic Press, New York, 1980.

[9] C. Guierull. Statistical analysis of multilook SAR interferograms for CFAR detection of ground moving targets. *IEEE Transactions on Geoscience and Remote Sensing*, 42(2):691–701, 2004.

[10] J. Jacobo-Berlles. *Nuevas Familias de Distribuciones Polarimétricas para Imágenes SAR*. PhD thesis, Departamento de Computación, Facultad de Ciencias Exactas y Naturales, Universidad de Buenos Aires, 2005.

[11] J. Jacobo-Berlles, M. Mejail, and A. C. Frery. The GA0 distribution as the true model for SAR images. In *Simpósio Brasileiro de Computação Gráfica e Processamento de Imagens*, Campinas, SP, Brazil, 1999. SBC, IEEE.

[12] J. Lee, M. Grunes, and G. de Grandi. Polarimetric SAR speckle filtering and its implication for classification. *IEEE Transactions on Geoscience and Remote Sensing*, 37(5):2363–2373, 1999.

[13] A. Lopès and F. Séry. Optimal speckle reduction for the product model polarimetric SAR imagery and the wishart distribution. *IEEE Transactions on Geoscience and Remote Sensing*, 35(3):632–647, 1997.

[14] G. Medioni and Y. Yasumoto. Corner detection and curve representation using curve B-splines. In *Proc. Conf. Computer Vision and Pattern recognitiont*, pages 764–769, 1986.

[15] M. Mejail, A. C. Frery, J. Jacobo-Berlles, and F. Kornblit. Approximation of the KA distribution by the GA0 distribution. In *Second Latinoamerican Seminar on Radar Remote Sensing: Image Processing Techniques*, pages 29–35, Santos, SP, Brazil, Sept. 1998. European Space Agency (ESA).

[16] M. Mejail, J. C. Jacobo-Berlles, A. C. Frery, and O. H. Bustos. Classificatiom of SAR images using a general and tractable multiplicative model. *International Journal of Remote Sensing*, 24(18):3565–3582, 2003.

[17] M. E. Mejail, A. C. Frery, J. Jacobo-Berlles, and O. H. Bustos. Approximation of distributions for SAR images: Proposal, evaluation and practical consequences. *Latin American Applied Research*, 31:83–92, 2001.

[18] K. Papathanassiou, T. Mette, and I. Hajnsek. Model based forest height estimation from single baseline polinSAR data: The fichtelgebirge test case. In *ESA POlInSAR workshop, ESRIN*, 2003.

[19] M. Quartulli and M. Datcu. Stochastic geometrical modelling for built-up area understanding from a single SAR intensity image with meter resolution. *IEEE Transactions on Geoscience and Remote Sensing*, 42(9):1996–2003, 2004.

[20] S. Quegan, M. Gomez-Dans, D. Gonzales-Sanpedro, D. Hoekman, T. Le Toan, and H. Skriver. Classification with multitemporal polarimetric SAR data. In *ESA POlInSAR workshop, ESRIN*, 2003.

[21] D. F. Rogers and J. A. Adams. *Mathematical Elements for Computer Graphics*. McGraw-Hill, New York, USA, 2 edition, 1990.

[22] S. J. S. Sant'Anna, A. H. Correia, C. C. Freitas, and A. C. Frery. The discriminatory capability of polarimetric SAR data for land use classification. In *International Geoscience and Remote Sensing Symposium: Remote Sensing of the System Earth – A Challenge for the 21st Century*, pages 1–3, Hamburg, Germany, 1999. IEEE, IEEE. CD-ROM.

[23] B. Scheuchl, I. Hajnsek, and I. Cumming. Sea ice classification using multi-frequency polarimetric SAR data. In *IGARSS'02*, Toronto, Canada, 2002.

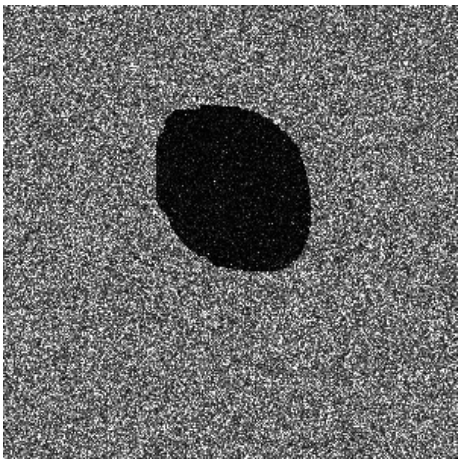

(a) HH Band

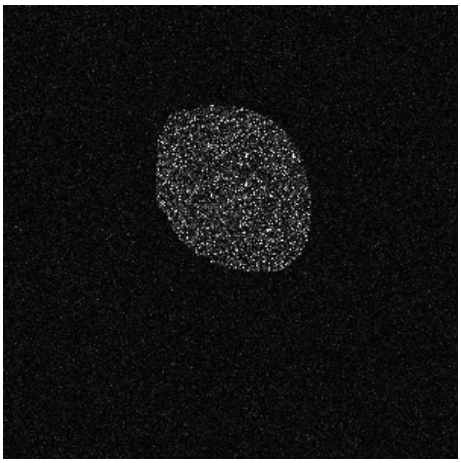

(b) HV Band

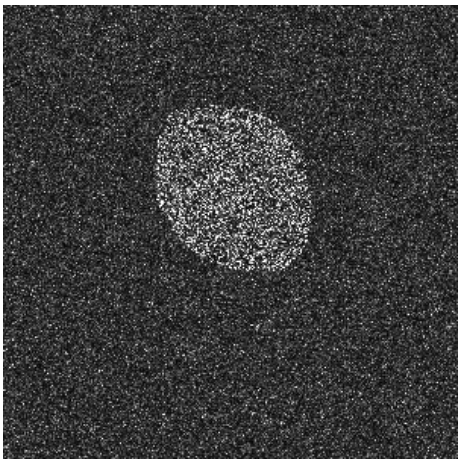

(c) VV Band

Figure 1. Syntethic polarimetric SAR image with two different regions for which the statistical parameters of the $\mathcal{G}^H$ distribution were estimated.

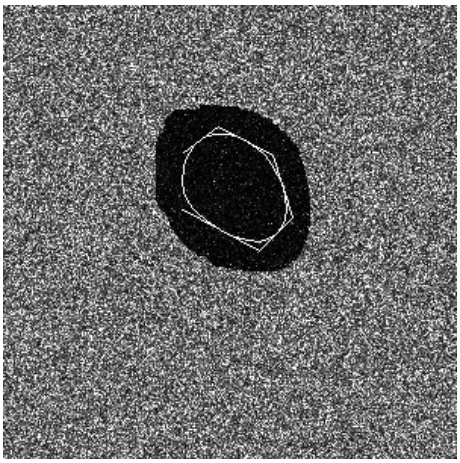

Figure 2. Initial Region specified by a polygon which vertexes generate a B-spline curve.

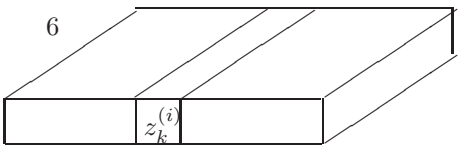

Figure 3. Scheme showing the data structure for segment $s^{(i)}$.

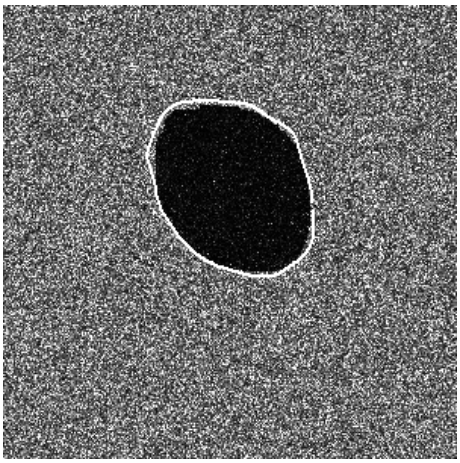

Figure 4. Synthetic image with the detected boundary.

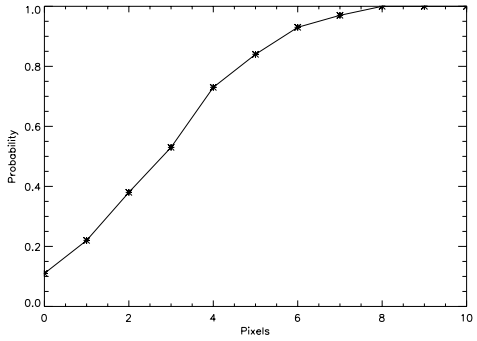

Figure 5. Probability of finding the transition point with an error lower than the one indicated on the horizontal axis, with the polarimetric $\mathcal{G}^H$ distribution.

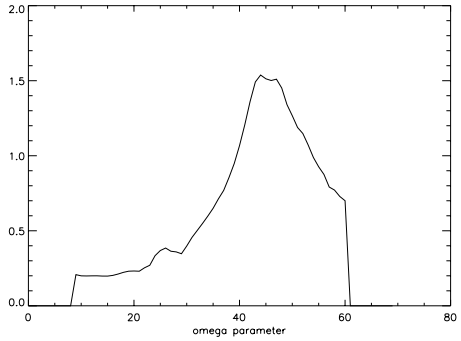

(a) Typical values

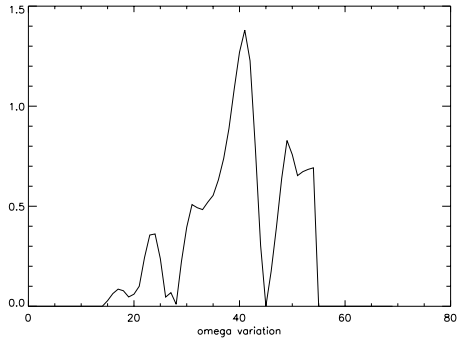

(b) Variation

Figure 6. Behavior of the parameter ω.

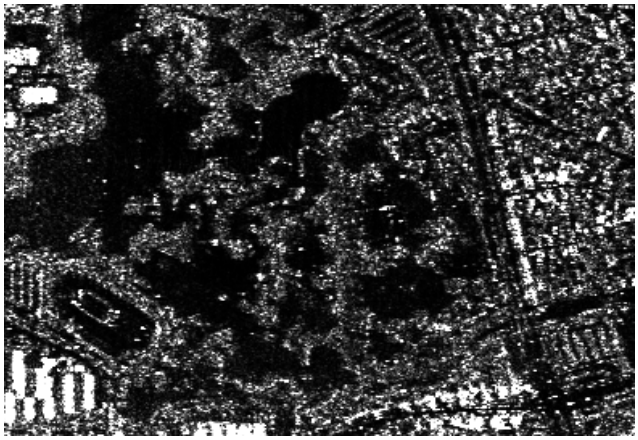

(a)

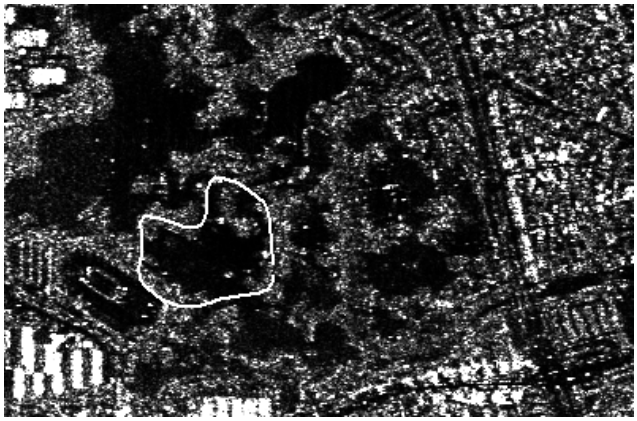

(b)

Figure 7. Real polarimetric three looks E-SAR image and boundary detection.